IAA-XX-14-16-05

Performance Analysis of a Double Discharge Pulsed Plasma Thruster by varying the Energy Distribution amongst its Two Stages

Luis Francisco Chrispim Marin*, Rodrigo Intini Marques**.

A Pulsed Plasma Thruster (PPT) is an electric space propulsion device mostly used for spacecraft orbit maintenance and attitude control. One of the most common issues with PPTs is the Late Time Ablation (LTA) - the sublimation of propellant that occurs after the main electric discharge, reducing propellant use efficiency. The Double Discharge PPT (DD-PPT) has two stages: The first stage works as a regular PPT and the second stage employs additional electric discharges to accelerate the first discharge plasma and the LTA. This work studied a DD-PPT and analyzed its efficiency and performance while varying the levels of energy employed on each of the two stages in order to archive maximum performance. A new electric circuit was designed to enable energy levels distribution amongst the two stages of the DD-PPT. An oscilloscope and a Rogowski current probe were used to estimate the impulse bit and a precision scale was used for measuring propellant mass variation. Inductance gradients were calculated using a mathematical model. Thruster tests were performed in a vacuum chamber with pressure of ~10^{-6} mbar. The results showed a significant increase in specific impulse. The optimum configuration of energy distribution occurred when a smaller percentage of the total energy was employed in the primary stage (for ablation) and a greater percentage of the total energy was employed in the second stage, used for plasma acceleration.

Nomenclature

b = primary electrode width, m

c = propellant exhaust speed with relation to the thruster, m/s

c_h = primary electrode height, m

d = secondary electrode width, m

d_e = distance between main axis of primary electrodes, m

d_0 = smaller width of secondary electrode, m

f = frequency of operation, Hz

h = distance between secondary electrodes, m

h_0 = smaller distance between secondary electrodes, m

l_e = length of secondary electrodes, m

l_x = maximum length with respect to the X axis of the secondary electrodes, m

m = rocket mass, kg

$\dot{m}$ = propellant mass flow rate, kg/s

m_p = propellant mass, kg

---

* MSc student at INPE- Brazilian National Institute for Space Research – LCP - Combustion and Propulsion Laboratory, chicomarin@lcp.inpe.br

** MSc supervisor and Researcher at INPE - Brazilian National Institute for Space Research – LCP - Combustion and Propulsion Laboratory, intini@lcp.inpe.br

$\dot{m}_p$ = propellant mass flow rate, kg/s

$\dot{v}$ = rocket velocity, m/s^2

x_p = axial distance from start of secondary electrodes, m

B = magnetic field, T

F = thrust, N

F_e = average magnetic thrust, N

F_g = local gravitational force, N

g_0 = gravitational acceleration at sea level, 9.807 m/s^2

I = current flowing through the plasma, A

J = current density, A/m^2

I_{bit} = impulse bit, Ns

I_{bit}^* = electromagnetic impulse bit, Ns

$I_{bit_p}^*$ = electromagnetic impulse bit produced by the primary electrodes, Ns

$I_{bit_s}^*$ = electromagnetic impulse bit produced by the secondary electrodes, Ns

$I_{bit_t}^*$ = total electromagnetic impulse bit, Ns

I_{sp} = specific impulse, s

I_{sp}^* = electromagnetic specific impulse, s

$I_{sp_p}^*$ = electromagnetic specific impulse (primary electrodes), s

$I_{sp_s}^*$ = electromagnetic specific impulse (secondary electrodes), s

$I_{sp_t}^*$ = total electromagnetic specific impulse, s

L' = electrode inductance gradient, H/m

L'_p = primary electrodes inductance gradient, H/m

L'_s = secondary electrodes inductance gradient, H/m

P_{in} = total electric power input, W

P_{jet} = ejected propellant kinetic power, W

η_p = primary stage efficiency, %

η_p^* = primary stage electromagnetic efficiency, %

η_t = total efficiency, %

η_t^* = total electromagnetic efficiency, %

α = angle between secondary electrodes, °

$\Delta\bar{L}$ = average inductance variation, H/m

Δm = mass ejected in a full discharge cycle (mass bit), kg

Δm_x = mass bit for configuration x

Δm_{1-4} = resulting mass bits for configurations 1-4

Δm_{5-8} = resulting mass bits for configurations 5-8

ε = total energy stored in the capacitors, J

ε_1 = energy stored in the capacitors of the primary stage, J

ε_2 = energy stored in the capacitors of the secondary stage, J

μ = magnetic permeability in vacuum, 1.2566×10^{-6} H/m

Introduction

1. Electric Propulsion

Space Propulsion is a means to change the momentum of a body in space. Rocket propulsion is a well-known type of space propulsion the produces thrust by ejecting propellant (matter stored in the space vehicle, also known as working fluid) [1]. Electric propulsion (EP) is a type of rocket propulsion that accelerates the propellant by electrical heating and/or by electric and/or magnetic body forces [2].

One of the advantages of EP is the possibility of achieving very high propellant exhaust velocity when compared to rockets using chemical propellants, allowing for a more efficient use of the working fluid [3]. Nowadays, the major disadvantage of EP is low thrust due to the lack of high power sources. Satellites that already provide high power to its subsystems (e.g., GEO telecommunication satellites) are the main candidates to employ EP in tasks as orbit transfer and maintenance and attitude control. The experience gained in near Earth applications of EP has encouraged its application in planetary and interplanetary missions [3] .

2. Pulsed Plasma Thruster (PPT)

A pulsed plasma thruster is an electric propulsion device that uses electric energy to ionize and electromagnetically accelerate the plasma to very high exhaust speeds [4], producing a high specific impulse [3] (up to 1200s [5] or more). An electric discharge ablates and ionizes a solid propellant, producing an arc plasma and the ions are then accelerated [5] by the Lorentz force. The solid propellant most commonly used is the Polytetrafluoroethylene (PTFE), known as Teflon™ [6].

The PPT is used as a propulsion device mainly for its intrinsic simplicity and reliability, even though it has a low total efficiency (around 10% or less) [7]. The PPT has been used in drag make up, orbit maintenance [7] and attitude control [8].

In a basic configuration, as shown in Fig. 1, the PPT is comprised of a solid propellant (PTFE), two electrodes (anode and cathode); a spring to feed the propellant; a power supply; a capacitor; and a spark plug [4]. The discharge between the electrodes occurs when a small amount of plasma produced by the spark plug [3] reaches the vicinity of the electrodes and acts as a mechanism that reduces the dielectric strength of the propellant. It then causes a breakdown and discharges the PPT capacitor [3] on the propellant surface in a high current (~kA) short duration (~μs) electric discharge current [4]. A small amount of the solid propellant sublimates and is ionized and accelerated electromagnetically [3].

One of the main issues with PPTs is the late time ablation (LTA) that is the propellant ablation that takes place after the main discharge is over, due to the propellant still being above the sublimation temperature. One solution for this problem is a variation of the PPT proposed by Intini-Marques [6], called the double discharge pulsed plasma thruster (DD-PPT).
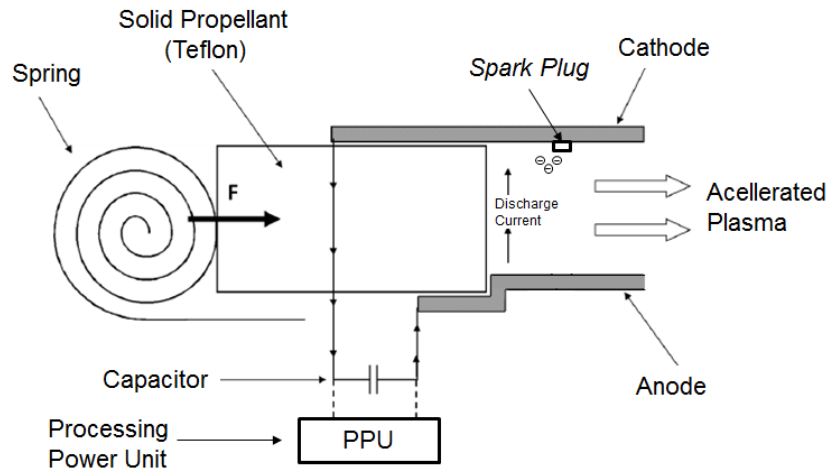
Fig. 1. A PPT diagram [6] [4] [3]

Double Discharge Pulsed Plasma Thruster

The DD-PPT is a way to address the LTA issue. The DD-PPT works by employing a second pair of electrodes downstream in order to accelerate the LTA. Another very important effect of employing a secondary pair of electrodes is the increase in specific impulse. In the DD-PPT, each pair of electrodes is called a stage and so the DD-PPT is comprised of two stages and that is a reason it is also called two-stage PPT or TS-PPT. Each stage is connected to its own capacitor. The first stage sublimates and accelerates the propellant. The second stage can further accelerate the propellant and/or the late ablation [6]. Figure 2 shows a diagram of a TS-PPT.
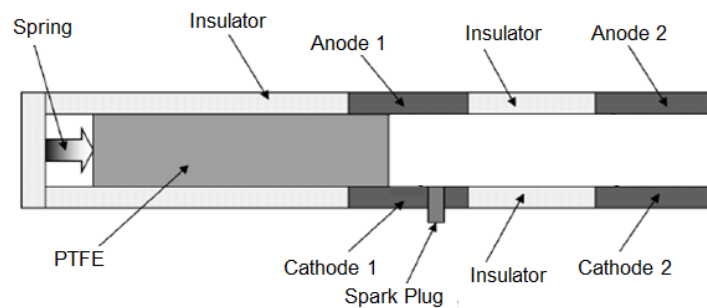
Fig. 2. A TS-PPT diagram adapted from [6].

The DD-PPT used in these tests was the one developed by Intini-Marques [6]. This DD-PPT has the secondary electrodes at an angle of 90 degrees in order to minimize carbon deposition on the surface of the structure that holds the electrodes [9]. Figure 3 shows a diagram of the DD-PPT and the built DD-PPT [10]. Table 1 shows the main design specification of the built DD-PPT.
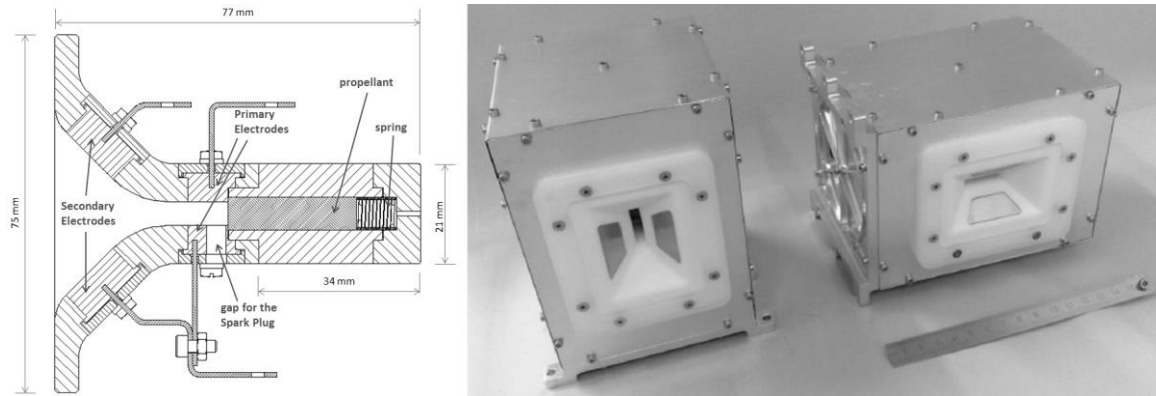
Fig. 3. DD-PPT – A diagram (left) and the built unit (right), adapted from **[10]**

DD-PPT parameter	Value
Total Mass	1.381 kg
Volume	152.5 x 113 x 128 (mm)
Maximum Power Consumption	4 W
Expected impulse for a 10 J total energy discharge	140 µNs
Maximum energy used in the primary stage	4.67 J
Maximum energy used in the secondary stage	4.59 J
Propellant Area exposed to the discharge	16 mm x 7 mm
Primary electrodes width	8.45 mm
Primary electrodes height	6 mm
Distance between primary electrodes mid-point axis	11 mm
Primary electrodes length	16.95 mm
Secondary electrodes thickness	7.2 mm
Angle between secondary electrodes	90°
Smallest distance between secondary electrodes	14.64 mm
Smaller width of secondary electrodes	20 mm
Bigger width of the secondary electrodes	35 mm
Length of the secondary electrodes	14 mm

Table 1. Main design specification of the built DD-PPT, adapted from **[9]**

DD-PPT Equations

Knowing the mass bit ejected in each pulse and analyzing the electric current curves of a PPT allows the inference of the electromagnetic impulse bit and electromagnetic specific impulse. The term electromagnetic is used because in this calculation we do not take into account the impulse produced by non-ionized propellant. This calculation method is useful when a thrust balance is not available and can give an insight of the performance parameters. The estimation of the impulse can be obtained with the following equation

$$I_{bit}^* = \frac{1}{2} \ L' \int \ I^2 \ dt \qquad [1]$$

where I_{bit}^* is the electromagnetic impulse bit and L' is the inductance gradient of the electrodes [11] [6].

The inductance gradient depends on the electrode geometry. For the primary stage (parallel, rectangular electrodes) the inductance gradient L'_p can be easily calculated using the literature [11]:

$$L'_p = 0,6 \ + 0,4 \ \ln \left(\frac{d_e}{b + c_h} \right) \qquad [2]$$

Where b is the width, c_h is the thickness [11] and d_e is the distance between the main axis of the electrodes [12].

The calculation of L' for the secondary electrodes is not as straight forward as they have an angle of 90 degrees between them and have trapezoidal shape, as shown in Fig. 3. As a starting point to calculate the average inductance gradient we used the method described by Schonherr, Herdrich, Roser e Auweter-Kurtz [13]:

$$\Delta \bar{L}(x_p) = \frac{\mu}{2\pi d} \int_0^{x_p} \int_0^d \int_0^h \frac{1}{d} \left\{ \left[\arctan\left(\frac{y}{z}\right) + \arctan(\frac{d-y}{z}) \right] \right.$$
$$\left. + \left[\arctan\left(\frac{y}{h-z}\right) + \arctan(\frac{d-y}{h-z}) \right] \right\} dz dy dx \qquad [3]$$

Where
$$h = h(x) = h_0 + 2 \ x \ tan(\frac{\alpha}{2}) \qquad [4]$$

$$d = d(x) = d_0 \left(1 - \frac{x}{l_e}\right) + d_e \frac{x}{l_e} \qquad [5]$$

The inductance gradient of the second stage is calculated taking into account the average inductance along the length of the electrode:

$$L'_s = \frac{\Delta\bar{L}(l_x) - \Delta\bar{L}(0)}{l_x} = \frac{\Delta\bar{L}(l_x)}{l_x} \qquad [6]$$

The calculated inductance gradients were calculated for the primary and secondary stages resulting in 0.491 µH/m for the first stage and 0.509 µH/m for the second stage.

The average electromagnetic thrust (F_e) represents the electromagnetic portion of the thrust due only to the Lorentz force. In order to find the average thrust we need to know the electromagnetic impulse bit and the thruster operation frequency (f):

$$F_e = f I^*_{bit} \qquad [7]$$

In order to calculate the specific impulse we need the mass bit Δm, wich is the mass ejected in a single discharge. This is obtained by weighting the propellant before and after many shots and then averaging the value for a single discharge. The average electromagnetic specific impulse I^*_{sp} can then be calculated:

$$I^*_{sp} = \frac{I^*_{bit}}{g_0 \Delta m} \qquad [8]$$

The total electromagnetic impulse of a single discharge is the sum of the electromagnetic impulse of the two stages [6]:

$$I^*_{bit_t} = I^*_{bit_p} + I^*_{bit_s} \qquad [9]$$

Using Equation [8] we can calculate the specific impulses of the primary $I^*_{sp_p}$ and secondary $I^*_{sp_s}$ stages:

$$I^*_{sp_p} = \frac{I^*_{bit_p}}{g_0 \Delta m} \qquad\qquad I^*_{sp_s} = \frac{I^*_{bit_s}}{g_0 \Delta m} \qquad [10]$$

The total electromagnetic specific impulse $I^*_{sp_t}$ of the DD-PPT is then calculated [6]:

$$I^*_{sp_t} = \frac{I^*_{bit_p} + I^*_{bit_s}}{g_0 \Delta m} = \frac{I^*_{bit_t}}{g_0 \Delta m} \qquad [11]$$

The electromagnetic total efficiency η^*_t is calculated as [6]:

$$\eta^*_p = \frac{1}{2} g_0 I^*_{sp_p} \left(\frac{I^*_{bit_p}}{\varepsilon_1}\right) \qquad\qquad \eta^*_t = \frac{1}{2} g_0 I^*_{sp_t} \left(\frac{I^*_{bit_t}}{\varepsilon_1 + \varepsilon_2}\right) \qquad [12]$$

Where ε_1 and ε_2 are the energy stored in the capacitors of the first and second stage, respectively.

Characterisation Method

The DD-PPT has two capacitor banks, one for each stage. The performance parameters change as the energy distribution amongst its two stages varies. Taking into account previous work [6] , different energy distribution configurations were defined and experiments were carried out to identify the best configuration. The experiment took place in a vacuum chamber at a pressure of 8×10^{-6} mbar and the discharges were monitored with Rogowski coils connected to an oscilloscope. For every configuration the DD-PPT discharged around 100 times. At the end of each configuration test the propellant was weighted in a precision scale to calculate the average mass bit ejected in every discharge.

1. *Performance Analysis of different energy distribution configurations*

With a voltage divider, it was possible to achieve different levels of energy on each stage by varying the voltage on the capacitor bank of each stage. Table 2 shows all the configurations tested. The reference energy for all tests is the maximum achievable total energy, which is 9.27 J. Table 2 shows two different energy distribution as percentages: one refers to the reference total energy available and another one refers to the distribution of the test total energy amongst the stages.

Configuration number	% of the maximum energy available first stage	% of the maximum energy available second stage	Energy first stage (J)	Energy of second stage (J)	Total energy (J)	Voltage primary stage (V)	Voltage secondary Stage (V)	% of the Test Energy distribution in the First Stage	% of the Test Energy Distribution in the Secondary Stage
1	50	0	4.67		4.67	849		100	0
2	50	29	4.67	2.70	7.38	849	592	63	37
3	50	35	4.66	3.27	7.93	848	670	59	41
4	50	50	4.67	4.59	9.27	849	850	50	50
5	29	0	2.71		2.71	592		100	0
6	29	29	2.70	2.70	5.41	592	592	50	50
7	29	36	2.72	3.35	6.08	594	679	45	55
8	29	49	2.71	4.57	7.28	592	848	37	63

Table 2. Energy distribution configuration

The tests were carried out at LCP - Combustion and Propulsion Laboratory - of INPE – The Brazilian National Space Research Institute on the facilities of the LPEL - Electric Propulsion Laboratory - on the BTSA - Altitude Simulation Test Bench - building using the equipment and resources listed on Table 3. Figure 5 shows the vacuum chamber and vacuum pumps used.

Resource	Description
DD-PPT thruster	Double discharge PPT built by Dr. Rodrigo Intini Marques
High precision scale	Mettler Toledo AT261 Delta Range Analytical Balance – precision of 10 µg.
Oscilloscope	TEKTRONIX TDS5034B Digital Phosphor Oscilloscope
Vacuum Chamber	Vacuum chamber in stainless steel with a volume 36,953 cm^3; Turbo-molecular pump Leybold TURBOVAC de 50000 rpm pumping capacity of 145 l/s and ultimate pressure of 10^{-10} mbar with controller Leybold TURBOTRONIX NT 150/360 VH; two-stage rotary pump TRIVAC B D8B pumping capacity 8 m^3/h; Pressure sensor BALZERS TP6300; pressure sensor EDWARDS Pirani 501;
Current Sensors	Two PEM CWT Rogowski Current Transducer;
Support, switching and protection systems developed for this project	Switching system to charge the capacitors and enable the discharge of the DD-PPT. Custom developed high voltage protection system for the DD-PPT power supplies. This system was developed with help from the LCP team and the MSc student Paula Fin.

Table 3. Equipment and resources
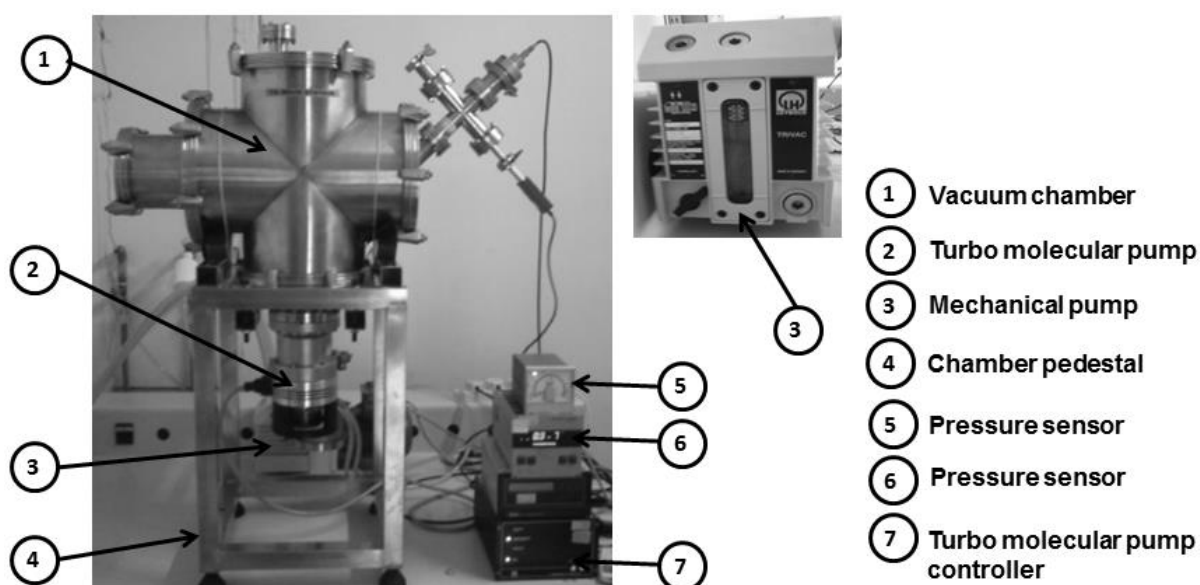
Fig. 4. Vacuum facility used for tests.

2. *Vacuum chamber tests*

Overall the DD-PPT discharged a total 975 times in 8 different configurations in a vacuum chamber with a pressure of 8.5×10^{-6} mbar. After testing each configuration the propellant was weighted to meas-

ure the propellant consumption. In order to calculate the impulse bit two Rogowski coils were surrounding the electrodes of both primary and secondary electrodes. The Rogowski coils were connected to their respective integrators that, in turn, were connected to a digital oscilloscope to store the current waveform that was later transferred to a computer to calculate the impulse bit. As an example, Fig. 6 shows the data acquired for energy configuration number 2. The output of the Rogowski coils is a voltage that must be converted to current, where 100 mV equals 1 kA.
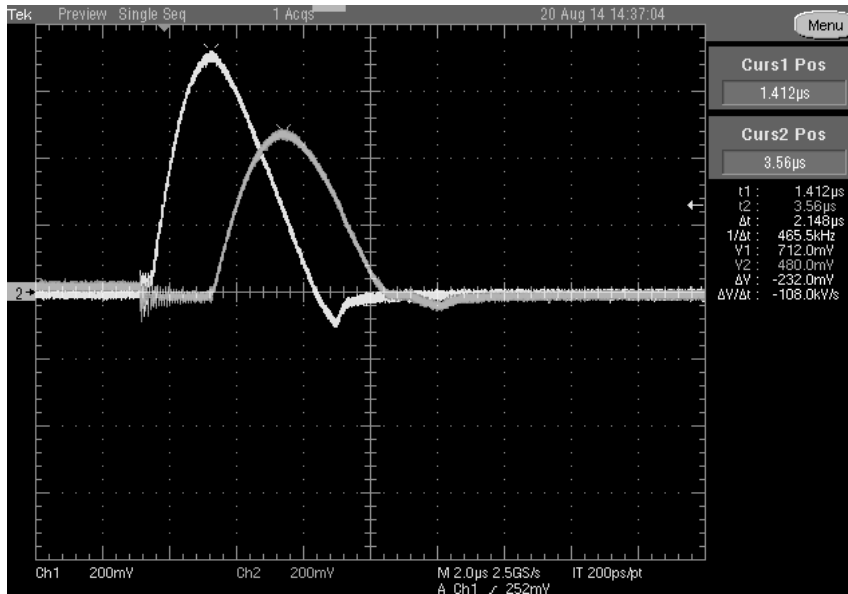
Fig. 5. Electric discharge signal from the integrator of the Rogowski coils.

From Fig. 5 we can see that the first stage has a peak current of 7.12 kA, as the signal from the integrator of the Rogowski coils reaches around 712 mV. After the plasma the reaches the second stage we can see that a current is flowing on the second pair of electrodes (oscilloscope channel 2), reaching around 4.8 kA. The whole event lasts around 8 µs. The discharge currents do not resemble a dumped sinusoidal shape [3] [6] as diodes were used to avoid current reversal in order to protect the capacitors.

3.   Results

The processed data acquired and converted to current measurements are summarized in Table 4 in a way that makes it ready for impulse bit calculations. By employing the mass bit averaged for each configuration, the equations shown and the method described, it was possible to calculate performance data, shown on Table 5 and visually displayed on Fig. 6.

Configuration number	% Energia Primeiro Estágio	% Energia Segundo Estágio	Integral I^2 Primeiro Estágio (A^2)	Integral I^2 Segundo Estágio (A^2)

1	50	0	120.33	0.00
2	50	29	104.01	52.04
3	50	35	99.59	61.92
4	50	50	99.78	90.16
5	29	0	67.64	0.00
6	29	29	59.58	49.37
7	29	36	55.47	70.81
8	29	49	64.17	92.53

Table 4. Data acquired converted to current and integrated over the discharge time.

Configuration Number	$I^*_{bit_p}$	$I^*_{bit_s}$	$I^*_{bit_t}$	$I^*_{bit_t}/\varepsilon$	Δm	$I^*_{sp_p}$	$I^*_{sp_s}$	$I^*_{sp_t}$	η^*_p	η^*_t
	(μNs)	(μNs)	(μNs)	(μNs/J)	(μg)	(s)	(s)	(s)	(%)	(%)
1	29.5	0.0	29.5	6.32	1.42	2125		2125	6.6	6.6
2	25.5	13.2	38.8	5.26	1.42	1837	953	2790	4.9	7.2
3	24.4	15.8	40.2	5.07	1.42	1759	1134	2893	4.5	7.2
4	24.5	22.9	47.4	5.12	1.42	1762	1651	3413	4.5	8.6
5	16.6	0.0	16.6	6.13	1.11	1524		1524	4.6	4.6
6	14.6	12.6	27.2	5.03	1.11	1342	1153	2495	3.6	6.1
7	13.6	18.0	31.6	5.20	1.11	1250	1654	2903	3.1	7.4
8	15.7	23.5	39.3	5.40	1.11	1445	2161	3606	4.1	9.5

Table 5. DD-PPT calculated performance parameters
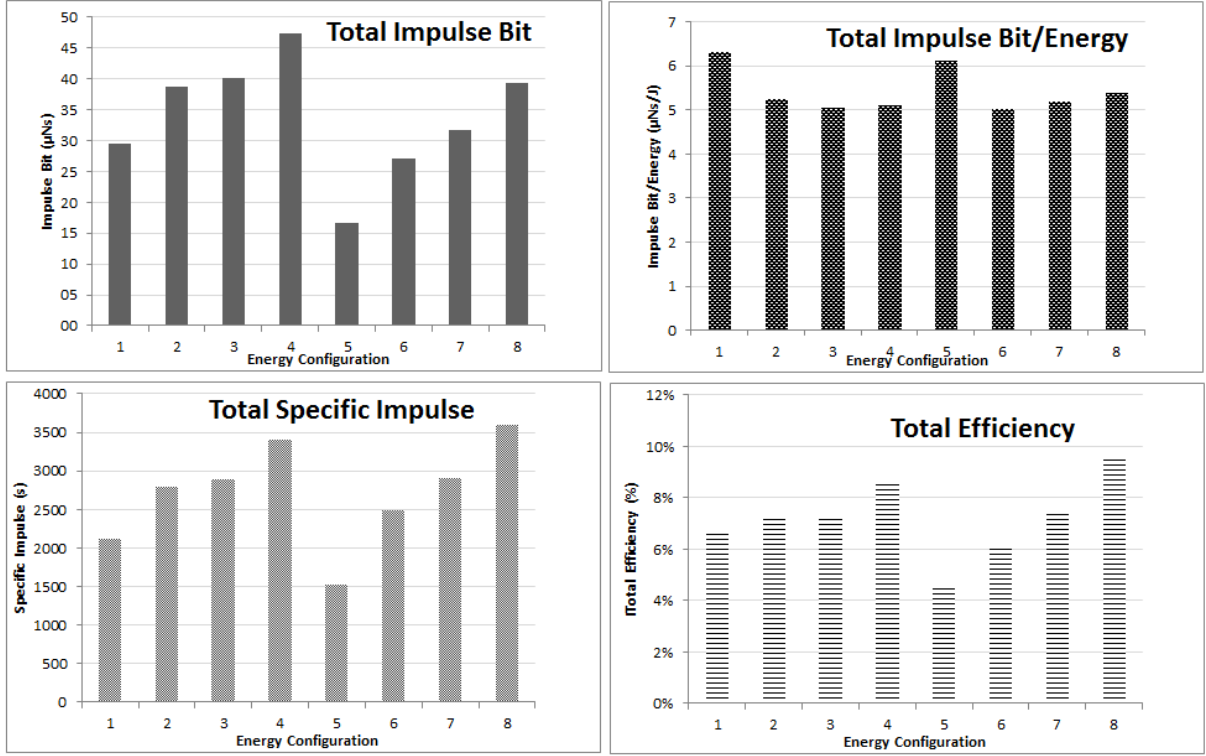
Fig. 6. Performance parameters comparison.

The mass bit Δm is not influenced by the second stage as it does not ablate mass [6]. Therefore, in order to increase the precision of the mass bit calculation, the averaged mass bit was calculated taking into account the energy of the first stage. As the configuration 1-4 had the same first stage energy discharge and the configurations 5-8 also had the same first stage energy discharge, it was possible to average the mass bit for these two cases, increasing the precision of the mass bit calculation:

$$\Delta m_{1-4} = \frac{\sum_{x=1}^{4} \Delta m_x}{4} \qquad [13]$$

$$\Delta m_{5-8} = \frac{\sum_{x=5}^{8} \Delta m_x}{4} \qquad [14]$$

The resulting mass bits for configurations 1-4, Δm_{1-4}, is 1.42 μg and the resulting mass bit, Δm_{5-8}, for configuration 5-8 is 1.11μg.

Analysis and Conclusion

In configurations 1 and 5 the DD-PPT works as a regular PPT, as there is no discharge in the second stage. In these configurations, we see that the first stage has a higher impulse bit than when the second stage discharges, even when the first stage has the same energy. The hypothesis raised is that due to the fact that the second stage produces a magnetic field opposite to the one on the first stage, it is creating a

detrimental effect on the first stage. While on a DD-PPT the main function of the first stage is mass ablation we would not like to have its performance decreased due to the use of a second stage. Therefore, a simple solution would be to invert the polarity of the second stage discharge so that the second stage can, instead, reinforce the magnetic field of the first stage discharge and further increase the impulse bit. This will be a subject of further investigation.

Overall, we can see that the impulse bit increases in direct proportion to the total energy employed and, with the exception of the configurations 1 and 5, all tests have a similar value of impulse bit produced per unit of energy, $I^*_{bit_t}/\varepsilon$, given to the thruster, around 5.1 µNs/J.

The specific impulse increases as the energy on the second stage increases. This is understandable as the energy on the second stage is used to further accelerate the plasma, keeping the mass bit constant. The configuration number 8 was chosen as the best performing one. This configuration had 37% of the test energy applied in the primary stage and 63% in the secondary stage and was the one with the highest specific impulse and efficiency and also the 3rd highest total impulse and impulse bit per unit of energy.

Further investigation on the overall performance of the DD-PPT is needed as the impulse bit per unit of energy achieved is below the expected value (10 µNs/J). We currently believe that the capacitor protection diodes used in this prototype may be dissipating part of the energy that would otherwise be used to accelerate the plasma. Further investigation about this issue is necessary.

Nevertheless, the DD-PPT tested was able to reach a maximum calculated specific impulse around 3600s, what is considered a significant increase over a regular PPT that would have a typical specific impulse of 1000s.

Future work include direct measurements of the impulse of the DD-PPT in order to take into account the thrust produced by the gas-dynamic contribution and also to confirm calculated performance data based on current measurements.

14

References

[1]   G. P. Sutton, O. Biblarz: Rocket Propulsion Element 7ed, 2001, page 1.

[2]   R. G. Jahn: Physics of Eletric Propulsion, 2001, pages 1-6

[3]   R. L. Burton, P. J. Turchi: Pulsed Plasma Thruster, 1998, Journal of Propulsion and Power, pages 716-720

[4]   R. J. Cassady, W. A. Hoskins, M. Campbell ,C. Rayburn: A Micro Pulsed Plasma Thruster (PPT) for the "Dawgstar" Spacecraft, 2000, in IEEE Aerospace Conference, page 2

[5]   D. M. Goebel, I. Katz: Fundamentals of Electric Propulsion: Ion and Hall Thruster, 2008, pages 1-28

[6]   R. M. Intini: A Mechanism to Accelerate the Late Ablation in Pulsed Plasma Thruster, 2009. Tese (PhD in ENGINEERING SCIENCES) - University of Southampton - Faculty of Engineering, Science & Mathematics - School of Engineering Sciences, pages 1-160

[7]   M. Keidar, I. D. Boyd, E. Antonsen, G. G. Spanjers: Electromagnetic Effects in the Near-Field Plume Exhaust of a Micro-Pulsed-Plasma Thruster, 2004, Journal of Propulsion and Power vol. 20 no 6, page 1

[8]   R. J. Vondra, K. I. Thomassen: Performance Improvements in Solid Fuel Microthrusters, 1972, AIAA 10th Aerospace Sciences Meeting - San Diego - California, page 738

[9] R. I. Marques, S. B. Gabriel, F. d. S. Costa: Progress on the design of a double discharge pulsed plasma thruster for the UniSat-5 satellite, 2008, 44th AIAA/ASME/SAE/ASEE Joint Propulsion Conference & Exhibit, Hartford USA, pages 4-5

[10] R. I. Marques, M. Street: Pulsed Plasma Pulsed - Project - Drawings by Mike Street - Concept by Rodrigo Intini Marques, 2007.

[11] R. L. Burton, M. J. Wilson,S. S. Bushman: Energy Balance and Efficiency of the Pulsed Plasma Thruster, 1998, in 34th AIAA/ASME/SAE/ASEE Joint Propulsion Conference and Exhibit AIAA-1998-3808 Cleveland OH , pages 5-8

[12] N. B. Standards: Radio Instruments and Measures, 1924, Circular of the National Bureau os Standards C74 Washington: United States Government Printing Office, page 246

[13] T. Schonherr, G. Herdrich, H.P. Roser, M. A. Kurtz: Influence of Electrode Shape on Performance of Pulsed Magnetoplasmadynamic Thruster SIMP-LEX, 2009, Journal of Propulsion and Power vol. 25, pages 382-383

Bibliografia a ser apagada antes de ser enviado.

[1]   G. P. Sutton e O. Biblarz, Rocket Propulsion Elemente 7ed, 2001.

[2]   R. G. Jahn, Physics of Eletric Propulsion, Mineola, New York: Dover Publications, INC, 2006.

[3]   R. L. Burton e P. J. Turchi, "Pulsed Plasma Thruster," *Journal of Propulsion and Power,* 1998.

[4]   R. J. e. a. Cassady, "A Micro Pulsed Plasma Thruster (PPT) for the "Dawgstar" Spacecraft," em *IEEE Aerospace Conference*, 2000.

[5]   D. M. Goebel e I. Katz, Fundamentals of Electric Propulsion: Ion and Hall Thruster, 2008, pp. 21-28.

[6]   R. M. Intini, "A Mechanism to Accelerate the Late Ablation in Pulsed Plasma Thruster," em *2009. 192f. Tese (PhD in ENGINEERING SCIENCES)*, University of Southampton - Faculty of Engineering, Science & Mathematics - School of Engineering Sciences, 2009.

[7]   N. e. a. Keidar, "Electromagnetic Effects in the Near-Field Plume Exhaust of a Micro-Pulsed-Plasma Thruster," *Journal of Propulsion and Power,* vol. 20, no. 6, 2004.

[8]   R. J. Vondra e K. I. Thomassen, "Performance Improvements in Solid Fuel Microthrusters," em *AIAA 10th Aerospace Sciences Meeting*, San Diego, California, 1972.

[9]   R. I. Marques, S. B. Gabriel e F. d. S. Costa, "Progress on the design of a double discharge pulsed plasma thruster for the UniSat-5 satellite," em *44th AIAA/ASME/SAE/ASEE Joint Propulsion Conference & Exhibit*, Hartford, CT, USA, 2008.

[10] R. I. Marques and M. Street, "Pulsed Plasma Pulsed - Project - Drawings by Mike Street - Concept by Rodrigo Intini Marques," 2007.

[11] R. L. Burton, M. J. Wilson e S. S. Bushman, "Energy Balance and Efficiency of the Pulsed Plasma Thruster.," em *34th AIAA/ASME/SAE/ASEE Joint Propulsion Conference and Exhibit, 1998. AIAA-1998-3808.*, Cleveland, OH , 1998.

[12] N. B. o. Standards, Radio Instruments and Measures - Circular of the National Bureau os Standards C74, Washington: United States Government Printing Office, 1924.

[13] T. Schonherr, G. Herdrich, H.-P. Roser e M. Auweter-Kurtz, "Influence of Electrode Shape on Performance of Pulsed Magnetoplasmadynamic Thruster SIMP-LEX," *Journal of Propulsion and Power,* vol. 25, Março 2009.